CrossMark

ALUMINUM: NEW ALLOYS AND HEAT TREATMENT

Modification of Al-Si Alloys by Ce or Ce with Sr

MARIO DE GIOVANNI,[1] JAMES A. KADUK,[2]
and PRAKASH SRIRANGAM[1,3]

1.—Warwick Manufacturing Group (WMG), University of Warwick, Coventry CV4 7AL, UK. 2.—Poly Crystallography, Inc., Naperville, IL 60540-5407, USA. 3.—e-mail: p.srirangam@warwick.ac.uk

Al-Si alloys were modified by addition of cerium (Ce) or Ce plus strontium (Sr) to study the effect on the eutectic silicon (Si) morphology. The modified alloys were characterized using scanning electron microscopy (SEM), x-ray diffraction (XRD) analysis, and thermal analysis to understand the effect of Ce and Sr on their microstructure. The results showed that addition of 1% Ce resulted in only partial modification of the Si phase, whereas addition of Ce with 0.04% Sr resulted in complete modification of the alloy. Addition of 1% Ce decreased the eutectic arrest temperature by about 10°C, compared with a 5°C drop with Sr addition only. SEM energy-dispersive spectroscopy (EDS) and XRD results revealed formation of Al_2Si_2Ce intermetallic in the Ce-modified Al-Si alloys. Differential scanning calorimetry (DSC) showed that the intermetallic formed just before the eutectic phase.

INTRODUCTION

Aluminum-silicon (Al-Si) alloys are widely used in the automotive and aerospace industries due to their high strength-to-weight ratio, good castability, and excellent mechanical and performance properties.[1] Slow solidification of such alloys produces a very coarse microstructure where the eutectic is composed of large plates or needles of Si in a continuous aluminum matrix. Alloys exhibiting this microstructure show low ductility due to the large and brittle Si plates. However, this coarse Si morphology can be modified into a fine and fibrous one by increasing the cooling rate or via chemical modification, improving the ductility and tensile strength of the alloy.[1,2] The first chemical modifier used industrially was sodium (Na). However, since the 1970s, the preferred modification element has been strontium (Sr), mainly due to its higher retention in the cast alloy and the lack of significant overmodification issues. Such microstructural modification can improve the mechanical properties, pressure tightness, and machinability, reduce the hot tear resistance, and significantly increase the fracture toughness of the alloy.[1–3]

Significant research has been carried out into the effect of various chemical elements, such as rare earths, for modification of Al-Si alloys.[4–9] Even though most rare-earth elements are chemically and crystallographically similar to strontium, their addition only results in refinement of the microstructure of Al-Si alloys. One such example is cerium (Ce). Previous research has shown that addition of 1% Ce to Al-Si alloys results in only partial modification of the Si morphology and an improvement in the mechanical properties of the alloy.[10] The Si morphology can be further refined by increasing the amount of Ce added to the alloy, whilst a fine fibrous structure can be obtained by combining Ce and chill casting.[9]

The mechanism by which such modification occurs has been greatly debated. Most theories focus on either growth-restriction-based mechanisms, mainly impurity-induced twinning (IIT),[11,12] or restricted growth[13] or nucleation-based effects, focusing on the formation of Al_2Si_2Sr (or similar) particles that deactivate eutectic Si nucleation sites.[14–16]

The aim of this work is to provide a basis to study the mechanistic differences between full modification, as achieved by using Sr, and the partial modification achieved by Ce. This is done by quantifying the modification achieved, characterizing the solidification of the alloys by thermal analysis, and identifying any intermetallics formed. The synergistic effect of combining Ce with Sr on the modification of the eutectic Si morphology in Al-Si hypoeutectic alloys is also investigated.

METHODOLOGY

Alloy Preparation

Al-Si hypoeutectic alloy was prepared by melting 99.999% purity Al (NewMet, UK) and 99.999% Si (Alfa Aeser, UK) in a clay graphite crucible using a Carbolite RHF1500 high-temperature furnace. Once the alloy was molten at 750°C, the metal was stirred using a graphite rod, poured into a preheated clay graphite crucible, and left to solidify. The cast Al-Si alloy was then used to prepare the modified alloys. The Al-Si alloy was remelted to allow for addition of Ce and Sr metals in the form of Al-10Ce (wt.%) and Al-10Sr (wt.%) master alloy. These alloys were poured into a preheated cylindrical graphite mold. The master alloys were produced similarly using the same 99.999% purity Al and 99% purity Sr (Alfa Aeser, UK) and 99.8% purity Ce (Alfa Aeser, UK), respectively. Four alloys were prepared with the following approximate compositions: Al-8 wt.%Si, Al-8 wt.%Si-0.04 wt.%Sr, Al-8 wt.%Si-1 wt.%Ce, and Al-8 wt.%Si-1 wt.%Ce-0.04 wt.%Sr. The chemical composition of each alloy was analyzed using inductively couple plasma optical emission spectroscopy (ICP-OES) (Supplementary Table SI). These concentrations of Ce and Sr in the alloys were chosen based on previous research and industrial practice.[2,9,10]

X-Ray Diffraction (XRD)

The unmodified and modified Al-Si alloys and master alloys were analyzed by XRD at Poly Crystallography Inc. (Naperville, USA) using a Bruker D2 Phaser diffractometer equipped with a LynxEye position-sensitive detector. The metal samples were mounted in a deep sample holder using modeling clay. The x-ray powder patterns were measured from 5° to 130° in steps of 0.0202144° at scan speed of 0.5 s per step, using a 0.6-mm divergence slit with 2.5° Soller slits and a 3-mm scatter screen height.

Microstructural Analysis

Metallographic samples for microstructural analysis were prepared from the cast cylinders by grinding and mechanical polishing. Etching was performed using a mixture of 20% hydrochloric acid (conc. 37%) and 80% isopropyl alcohol to reveal the fibrous or lamellar structure of the Si eutectic. The analysis was carried out by means of optical microscopy and on a Zeiss-Sigma field emission gun-scanning electron microscope (FEG-SEM). Quantitative dimensional analysis of the Si phase was performed by analyzing five images acquired by SEM at × 5k, using ImageJ 1.50i software. Chemical analysis was performed using energy-dispersive spectroscopy (EDS). The electron backscatter diffraction (EBSD) capability of the same SEM was also used to elucidate the grain misorientations in primary and eutectic Al.

Thermal Analysis

The progress of solidification in the four samples was analyzed by examining their respective cooling curves. Approximately 15 g of each sample were placed in a clay graphite crucible and melted at 750°C in an electrical resistance furnace. Once molten, the crucible was taken out and a K-type thermocouple was immediately inserted below the surface of the melt. The cooling curve was collected using a data logger recording at 10 Hz. Under these conditions, a cooling rate of 1.2 ± 0.2°C/s was observed. The measurement was repeated to ensure repeatability.

Differential Scanning Calorimetry (DSC)

Thermal analysis by means of DSC was conducted on the prepared alloys using a Netzsch STA 449 F3 Jupiter to determine the phase changes taking place. These experiments were conducted in inert argon (Ar) atmosphere at heating and cooling rate of 10 K/min, repeating the melting–solidification cycle for three times. Due to the overlapping peaks of the eutectic and primary Al, the peaks were plotted using OriginPro® 2016 (64-bit) b9.3.226 and bi-Guassian multiple peak fit analysis was carried out to obtain the eutectic onset temperature.

RESULTS AND DISCUSSION

X-Ray Diffraction Analysis

Figure 1 presents the XRD spectra of the four alloys under investigation and the master alloys from which they were produced. The peaks of interest in each spectrum are indicated with an asterisk, except in Al-Si, where the Al and Si peaks are differentiated using an asterisk and a circle, respectively. Figure 1a, b, and c shows the spectra for Al-Si, Al-Sr, and Al-Si-Sr. The spectrum for Al-Si-Sr is identical to that for Al-Si, thus yielding no information with respect to whether Al_4Sr is still present in the alloy or whether a ternary intermetallic phase formed. However, previously published research demonstrated that Al-Si-Sr ternary intermetallic particles form in this specific alloy and constitute 0.03% by volume of the alloy.[17] The lack of a peak for this component in Fig. 1c is due to the extremely small amount of Sr added in this alloy.

Figure 1d, e, and f presents the XRD spectra for Al-Ce, Al-Si-Ce, and Al-Si-Ce-Sr. The dominant phase in Al-Ce was $Al_{11}Ce_3$, changing to Al_2Si_2Ce when Al-Ce was added to Al-Si. Previous research has indicated that Al_2Si_2Ce is a metastable phase and that the thermodynamically favored phase at similar compositions would be $AlSi_2Ce$.[18] However, the XRD results seem to indicate that, under these casting conditions, the metastable Al_2Si_2Ce forms.

When compared with the Sr addition in Al-Si-Sr, the amount of Ce added in Al-Si-Ce and Al-Si-Ce-Sr is much greater, thus the amount of intermetallics formed is also significantly increased. The spectra
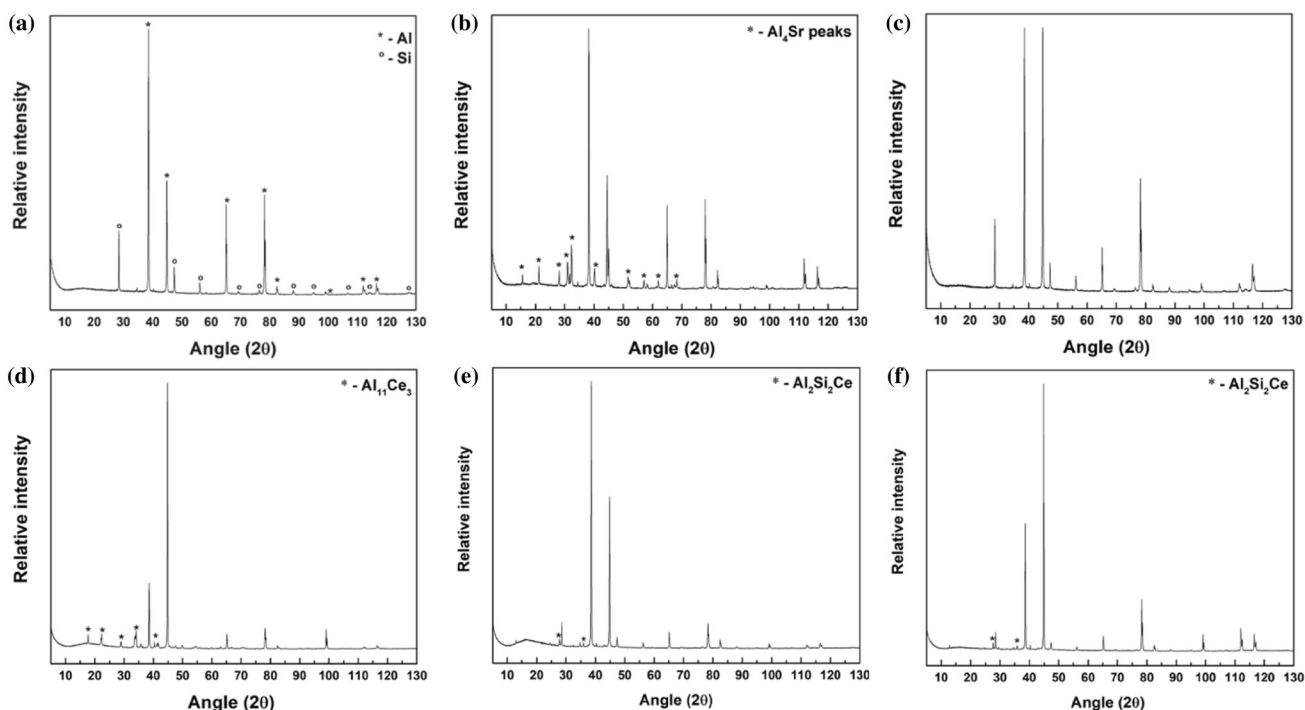
Fig. 1. XRD spectra of (a) Al-Si, (b) Al-Sr, (c) Al-Si-Sr, (d) Al-Ce, (e) Al-Si-Ce, and (f) Al-Si-Ce-Sr.

for Al-Si-Ce and Al-Si-Ce-Sr are identical, indicating that XRD is unable to identify the presence of any new particles formed or changes to the Al_2Si_2Ce due to the Sr addition.

Microstructural Characterization

Figure 2a, d, g, and j shows optical microscopy images of the unmodified and modified alloys. In Fig. 2a, the unmodified alloy shows primary Al and eutectic Si in the form of elongated plates, whilst Fig. 2d shows the Sr-modified alloy, where addition of Sr resulted in modification of the eutectic Si to a fine fibrous structure. Figure 2g shows that addition of 1% Ce caused refinement of the eutectic Si compared with the unmodified condition. The combined effect of Ce and Sr is shown in Fig. 2j, where the eutectic Si closely approaches full modification to a fine fibrous structure, though some longer Si features can be observed. In the alloys containing Ce, large block-like features, indicated by an arrow, can also be noted. These are Ce-containing intermetallics which form in the alloy.

Figure 2 also shows SEM images of the polished (b, e, h, k) and etched (c, f, i, l) alloy samples. The images obtained from the polished samples can be considered as a high-magnification version of the optical images. Note that the Si in the Al-Si (b) alloy is present in a flake-like structure, whilst the Al-Si-Sr (e) and Al-Si-Ce-Sr (k) show very similar microstructures, i.e., a fine fibrous one. On the other hand, the Al-Si-Ce (h) sample shows a partially modified microstructure, as both flake-like and fiber-like Si can be observed. The etched

samples provide further understanding on the microstructural modification by imaging the Si at subsurface level. The Si flake-like structure of Al-Si is confirmed in Fig. 2c. The fine fibrous Si microstructure in Al-Si-Sr and Al-Si-Ce-Sr can also be seen in Fig. 2f and l, respectively. These images indicate an almost identical Si morphology in both of these alloys. Further insight is provided for Al-Si-Ce in Fig. 2l, which shows a central flake-like feature in the shape of an "X" surrounded by fibers. This confirms that 1% Ce only partially modified the Si phase, as observed in previous studies.[4,9,10]

The modification effect in the different alloys was analyzed quantitatively in terms of the Feret diameter and circularity by analyzing five SEM images. It must be clarified that this quantitative analysis was performed on a two-dimensional (2D) cross-section and thus yields information regarding the apparent size and shape of the Si eutectic in this plane. The Feret diameter is defined as the longest distance between any two points along the selection boundary.[19] The circularity is defined as $4\pi \times \frac{\text{Area}}{\text{Perimeter}^2}$, where a value of 1 indicates a perfect circle, with decreasing values indicating less circular features.[19] Alloys presenting shorter and more circular Si features can be considered to have achieved a higher degree of modification. The results of this analysis are presented as histograms in Fig. 3. Figure 3a shows the Feret diameter distribution of the Si features across the whole range, while the inset zooms in on the region from 0 μm to 2 μm. Figure 3b shows the circularity
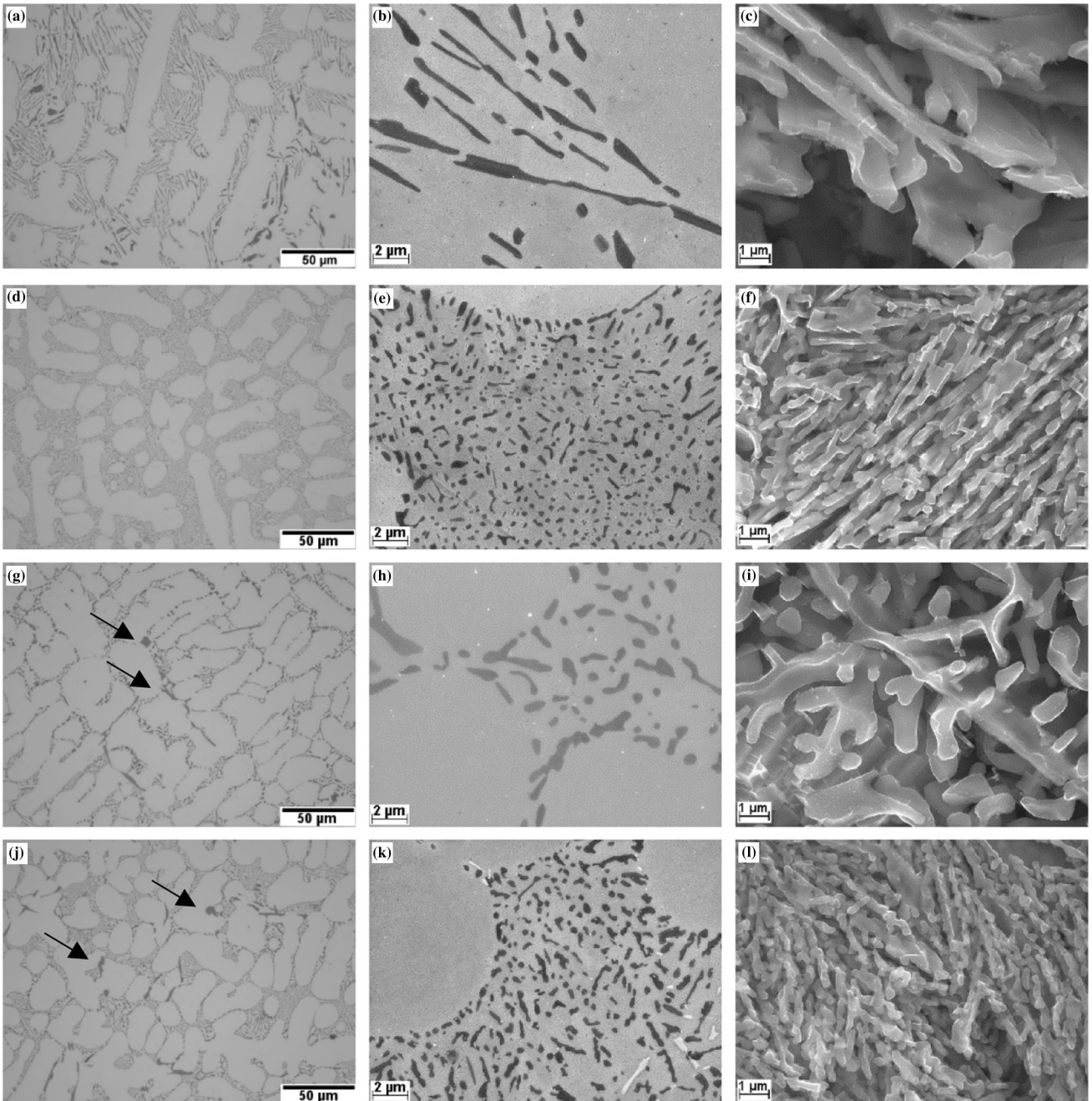
Fig. 2. Optical microscopy images (a, d, g, j) and scanning electron microscopy images on unetched (b, e, h, k) and etched (c, f, i, l) samples of Al-Si (a–c), Al-Si-Sr (d–f), Al-Si-Ce (g–i), and Al-Si-Ce-Sr (j–l).

distribution of the Si phase. Tabulated data are also shown as insets to these figures.

Figure 3 shows a distinct trend between the two alloys that contain Sr and the two that do not. Al-Si-Sr and Al-Si-Ce-Sr both present Si features with markedly smaller average Feret diameter and higher average circularity, indicating that a significantly higher degree of modification was achieved. Al-Si showed slightly longer and significantly less circular Si features compared with Al-Si-Ce, indicating that addition of 1% Ce partially modified the

Si within the microstructure. On the other hand, the two Sr-containing alloys presented similarly sized and shaped Si. A slight difference in the circularity of these alloys can be observed in Fig. 3b. Al-Si-Ce-Sr seemed to show a slightly higher percentage of features with lower circularity (< 0.8) compared with Al-Si-Sr. Though only marginal, this could be further confirmation of the observations made based on the SEM microstructures, i.e., the presence of longer features in Al-Si-Ce-Sr compared with Al-Si-Sr.
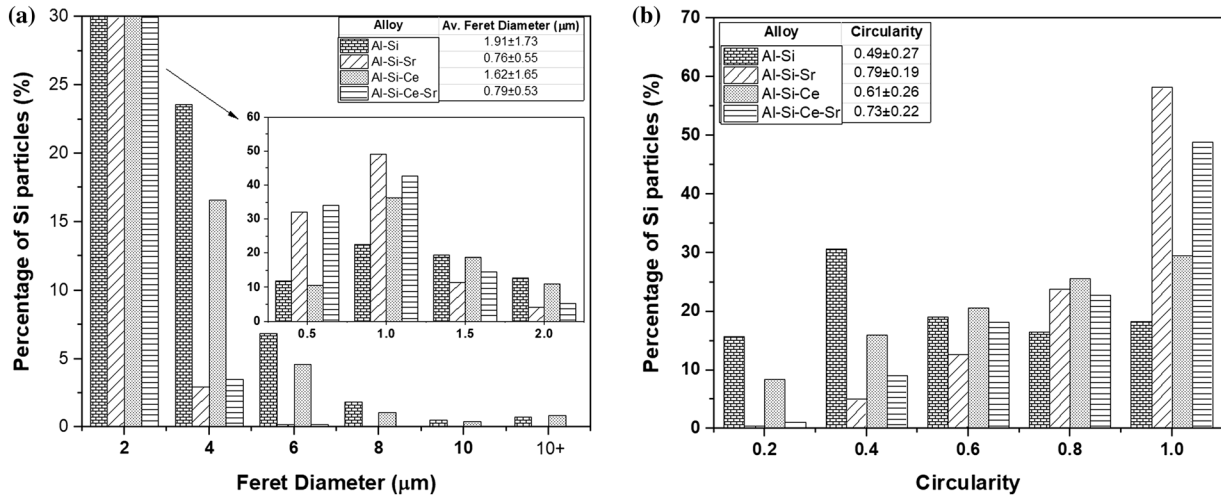
Fig. 3. (a) Size distribution analysis of the Si phase comparing Al-Si, Al-Si-Sr, Al-Si-Ce, and Al-Si-Ce-Sr, (b) shape distribution analysis for the same alloys. The table insets show average values and standard deviation for the alloys.

Thermal Analysis

Figure 4 shows the eutectic region of the cooling curves for each of the four different alloy compositions. The complete cooling curves are provided in Supplementary Fig. S1. The nucleation temperature (T_N), minimum temperature (T_{MIN}), growth temperature (T_G), and recalescence ($T_G - T_{MIN}$) were measured. The eutectic T_N is the point at which Si crystals start to nucleate. It can be extracted from the cooling curves by plotting the derivative of the curve and reading out where the tangents of the two slopes meet. T_{MIN} is the point where the eutectic Si and Al have grown to a stage where the latent heat evolved during the growth process balances the heat flow out of the system. T_{MIN} leads to recalescence, which takes place when the release of latent heat exceeds the heat extraction from the system. This results in a new heat balance, which is denoted as T_G.[20] These results show that addition of 1% Ce extended the mushy zone, as the primary growth temperature increased whilst the eutectic arrest temperature decreased. This allows for further growth of primary Al. The eutectic nucleation decreased by 5°C upon adding 400 ppm Sr. Upon adding 1% Ce, the nucleation temperature was depressed by a further 5°C, whereas upon addition of both Ce and Sr, the nucleation temperature increased by about 2°C in comparison with addition of 1% Ce only. The depression of the eutectic growth temperature is frequently regarded as an indication of the microstructural modification obtained. This is normally attributed to the aluminum phosphide (AlP) nucleation sites becoming poisoned by the modifying element, causing eutectic nucleation to occur at a lower temperature. However, in this case, note that the depression of the eutectic growth temperature does not reflect the microstructural modification obtained. This has also been observed by other
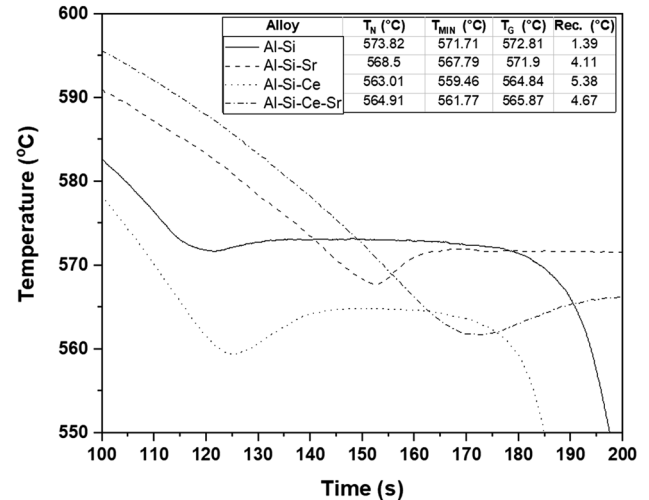

Fig. 4. Comparison of the eutectic region of the cooling curves of Al-Si, Al-Si-Sr, Al-Si-Ce, and Al-Si-Ce-Sr.

authors when adding rare-earth elements to Al-Si alloys.[10,20,21] There is also a marked difference in the eutectic recalescence, which increased from 1.4°C for unmodified Al-Si to approximately 5°C in presence of Ce, in both Al-Si-Ce and Al-Si-Ce-Sr. The depression in the eutectic growth temperature, for all three modified alloys, seems to indicate that Al_2Si_2X compounds, where X could be either Ce or Sr, deactivates any AlP from acting as nucleating sites for the eutectic. The greater extent to which the eutectic growth temperature is affected in the Ce-containing alloys may be related to their higher Ce content. The lack of nucleation sites and therefore more homogenous nucleation is shown by the smaller but nevertheless flake-like Si structure. Therefore, the decrease in eutectic growth can be related to the removal of nucleation sites and more homogenous nucleation, but not to the

morphological transition to a fiber-like eutectic observed in the presence of Sr. Furthermore, note that supercooling $(T_{\mathrm{G}} - T_{\mathrm{N}})$ was observed for all the alloys, except the unmodified alloy. Hanna et al. showed that supercooling occurs in hypoeutectic Na-modified Al-Si alloy but not in unmodified alloy, indicating that the modification affects the nucleation of eutectic Si.[22] The fact that the same effect can be seen in Al-Si alloys containing both Sr or Ce indicates that both of these elements affect the nucleation of eutectic Si.

Differential Scanning Calorimetry

DSC was primarily used to identify the temperature of formation of any intermetallic phases, since no indication of these was observed in the cooling curves. DSC was also used as a cross-check for the trends observed in the cooling curves. Figure 5 shows the second cooling cycle during the DSC analysis of the different samples. The inset table presents the average and standard deviation of the primary and eutectic onsets for the three cooling cycles. Note from the DSC curves that, for all the modified alloys, the primary onset occurred much earlier. This is similar to what was observed in the cooling curves, though it is more evident now, due to the slower cooling rates. The interpretation of the eutectic onset is more difficult, as it overlaps with the primary onset. Bi-Gaussian curve fitting was performed, and the first deviation from the baseline of the eutectic curve was extracted as the eutectic onset.

One of the first observations is that the eutectic onset for the unmodified Al-Si occurred at 587°C rather than the well-known equilibrium eutectic temperature of 577°C. This indicates that the curve fitting used here can only be used to correlate trends between the alloys being analyzed rather than for comparison with more general, absolute values. Nonetheless, for all the modified samples, the eutectic onset occurred at a much lower temperature than for the unmodified sample. The Sr-modified sample exhibited a eutectic onset temperature similar to the Ce-containing samples. This contrasts with the cooling curve data, where the eutectic nucleation temperature was significantly higher for Al-Si-Sr compared with Al-Si-Ce or Al-Si-Ce-Sr. For the Ce-containing samples, an inflection occurred at the beginning of the eutectic formation, being more evident for Al-Si-Ce. This difference between the results of the two techniques can be attributed to the inflection in the curve. In fact, comparison of the peak position shows that, for the Ce-containing samples, the peak occurs at a much later stage than for Al-Si-Sr. This inflection is attributed to the formation of intermetallics in the alloy.

It was also generally observed that samples containing Sr showed lower standard deviation than the other alloys. During this analysis, it was noted that minimal oxidation occurred on the Sr-containing samples, which retained their shiny appearance, indicating that, under these conditions, a thick oxide layer did not form. On the other hand, the alloys that did not contain Sr turned dull, indicating formation of an oxide layer. This oxide formation explains the drift from the first to third cycle and the higher standard deviation for the alloys that did not contain Sr.

A number of authors previously employed DSC to measure the undercooling in Al-Si, using melt-spun alloys. In such cases, two distinct peaks formed for the eutectic formation, the first representing solidification of eutectic Si along grain boundaries and the second representing solidification of entrained eutectic Si within the Al matrix.[23,24] In some cases, when exploring the effect of addition of trace amounts of modification elements such as strontium and europium, detection of intermetallic compound formation was also achieved, appearing as a small peak just after the first eutectic peak.[25,26] In this study, intermetallic formation was detected just at the start of the eutectic formation. The addition of Sr to Al-Si-Ce also seems to bring the intermetallic formation forward slightly.

Energy-Dispersive Spectroscopy

EDS chemical composition maps for the Al-Si and Al-Si modified alloys were acquired and are presented in Supplementary Fig. S2, clearly showing the segregation of Al and Si in their respective phases. Furthermore, they show that, in the presence of Ce, intermetallic phases made up of all three elements formed. For Al-Si-Sr and Al-Si-Ce-Sr, the Sr map is also presented, although its concentration within these areas was too low to be detected. The presence of Al_2Si_2Sr intermetallics in Al-Si-Sr has been previously shown by EDS and quantified by x-ray computed tomography (XCT).[17]

These results show that, in such systems, ternary intermetallic compounds in the form of Al_2Si_2X form as an intrinsic part of the solidification process. Previous research has debated the formation of Al_2Si_2Sr as a crucial aspect of the nucleation and subsequent modification of the eutectic Si.[16,27] The formation of Al_2Si_2Ce and the lack of full modification in the Al-Si-Ce alloy indicate that the formation of such compounds is not a crucial factor in predicting the modification potential of an element. Some authors have debated whether the formation of nanoclusters, with different shapes, of Al_2Si_2Sr within eutectic Si is the contributing factor for the modification potential of Sr.[28,29] Therefore, further work, by means of transmission electron microscopy and atom probe tomography, is required to fully characterize the eutectic Si partially modified by Ce, and to explore whether such nanoclusters also form after addition of Ce.
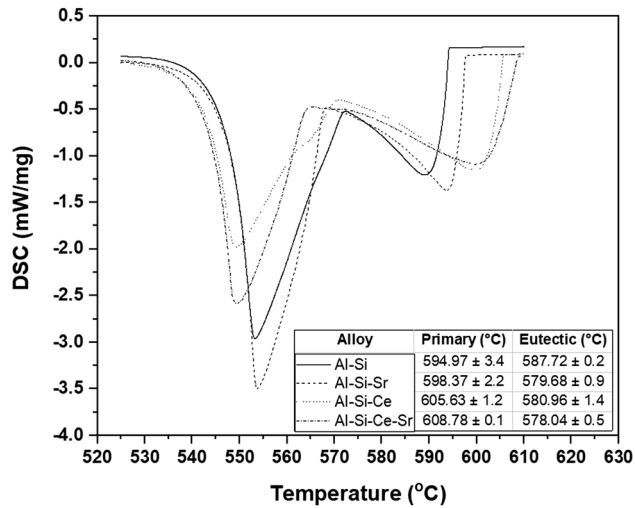
Fig. 5. Comparison of the second cooling cycle in DSC analysis of Al-Si, Al-Si-Sr, Al-Si-Ce, and Al-Si-Ce-Sr.

Electron Backscatter Diffraction

Large-area EBSD misorientation maps were acquired on the four alloys and are presented in Supplementary Fig. S3. Different grain colors indicate misorientation greater than 5°. From these maps it can be noted that, in unmodified Al-Si, the primary Al dendrite orientation extends within the eutectic Al. This indicates that the solidification of the eutectic Al occurred mainly on primary Al dendrites. There are also some areas in the Al-Si map that seem to have nucleated separately from the primary dendrite, but when comparing the Al-Si EBSD map with the Al-Si-Sr one, a stark contrast can be noted immediately. The latter shows complete separation between the primary and eutectic Al, as individual areas within the eutectic have different orientations relative to each other and relative to the primary. In the Al-Si-Ce and Al-Si-Ce-Sr alloys, though not as evident primarily due to
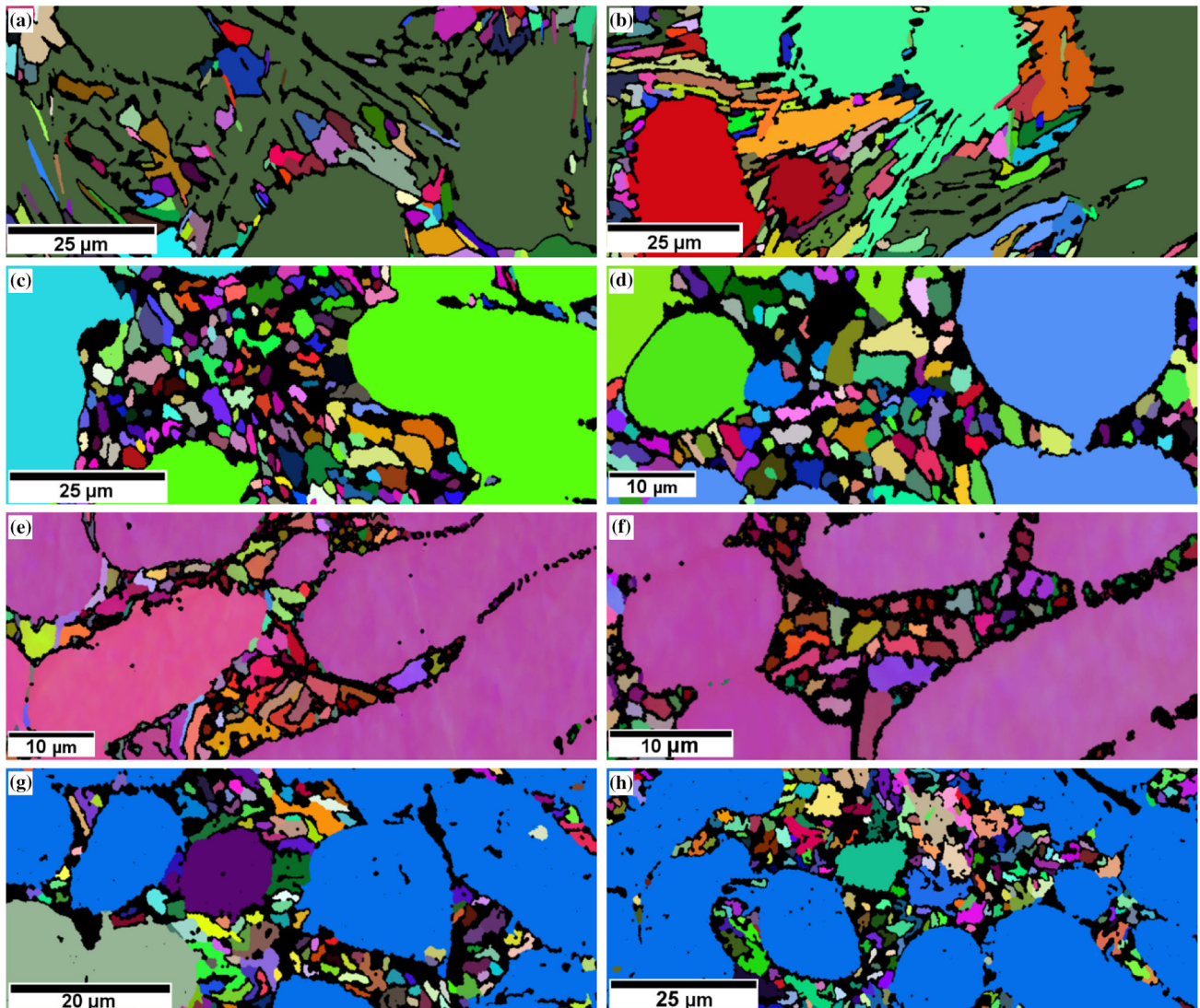

Fig. 6. EBSD maps for (a, b) Al-Si, (c, d) Al-Si-Sr, (e, f) Al-Si-Ce, and (g, h) Al-Si-Ce-Sr. (Color figure available online).

the smaller eutectic region, a similar observation can be made.

Magnified images from different regions of each EBSD map are provided in Fig. 6, as these provide more detailed information. Images from the Al-Si map are shown in Fig. 6a and b. Note that most of the eutectic Al region has the same orientation as the primary Al in proximity (dark green in a, bright green in b). However, there are also grains which show a misorientation from the primary Al.

EBSD has been previously employed to shed light on the solidification behavior of Sr-modified and unmodified Al-Si alloys.[14,30–33] Most of this research explored the Al solidification. Nogita and Dahle[30] argue that, if the eutectic Al nucleates on the primary Al dendrite, the orientation of the eutectic Al would be the same as that of the primary dendrite, whereas if the eutectic Al nucleates in the interdendritic liquid, the orientation would be different from that of the primary Al dendrite. Their results indicated a transition from the former to latter mechanism upon modifying alloy 319 with 70 ppm Dahle et al.[14] agreed with this observation, but noted that, at higher levels of Sr, the eutectic Al growth reverted back to growth in the same orientation as the primary Al dendrite whilst still achieving complete modification of the Si phase. Heiberg and Arnberg[32] noted the same mechanism when using high-purity alloys modified with 150 ppm Sr. The results presented herein indicate a general trend which shows that, in the presence of Ce and/or Sr, the solidification of the eutectic Al occurs independently from the primary Al dendrite, as individual eutectic Al regions have different orientations with respect to the primary Al.

CONCLUSION

- Addition of 1% Ce caused partial modification of Al-Si. Upon addition of 0.04% Sr to Al-Si-Ce, full modification was obtained, being comparable to the Sr modification employed industrially.
- Cooling curves and DSC results showed that the primary Al growth temperatures were increased in the presence of 1% Ce.
- Cooling curves and DSC results showed that the eutectic nucleation and growth temperatures were reduced. It is also noted that, in the presence of 1% Ce, the eutectic growth temperature was significantly lower than in the unmodified or Sr-modified Al-Si. Although this is normally regarded as an indication of the modification effect, microstructural examination of the Al-Si-Ce alloy showed otherwise.
- Addition of Ce caused formation of an intermetallic phase, identified as Al_2Si_2Ce by means of XRD and EDS.
- EBSD indicated that, in the presence of Ce and/or Sr, the solidification of the eutectic Al was completely independent of the primary Al. The

fact that Ce and Sr, a partial and full modifier, respectively, showed the same behavior indicates that the solidification of the eutectic Al in relation to the primary Al is not a contributing factor to the modification of the Si eutectic phase.

ELECTRONIC SUPPLEMENTARY MATERIAL

OPEN ACCESS

REFERENCES

1. I.J. Polmear, *Light Alloy* (Amsterdam: Elsevier, 2005), pp. 205–235.
2. R. Bartley, *British and European Aluminium Casting Alloys* (Birmingham: Association of Light Alloy Refiners, 1996).
3. J.E. Hatch, *Aluminium: Properties and Physical Metallurgy*, 2nd ed. (Materials Park: American Society of Metals, 1984).
4. K. Nogita, S.D. McDonald, and A.K. Dahle, *Mater. Trans.* 45, 323 (2004).
5. B.J. Ye, *Trans. Am. Foundrymen's Soc.* 93, 533 (1985).
6. Z. Shi, Q. Wang, Y. Shi, G. Zhao, and R. Zhang, *J. Rare Earths* 33, 1004 (2015).
7. H. Qiu, H. Yan, and Z. Hu, *J. Alloys Compd.* 567, 77 (2013).
8. Y.C. Tsai, C.Y. Chou, S.L. Lee, C.K. Lin, J.C. Lin, and S.W. Lim, *J. Alloys Compd.* 487, 157 (2009).
9. V. Vijeesh and K.N. Prabhu, *Light Metals 2015* (Hoboken: Wiley, 2015), pp. 403–407.
10. Y.C. Tsai, S.L. Lee, and C.K. Lin, *J. Chin. Inst. Eng.* 34, 609 (2011).
11. S. Lu and A. Hellawell, *J. Cryst. Growth* 73, 316 (1985).
12. S.-Z.S. Lu and A. Hellawell, *Metall. Trans. A* 18, 1721 (1987).
13. K.F. Kobayashi and L.M. Hogan, *J. Mater. Sci.* 20, 1961 (1985).
14. A.K. Dahle, K. Nogita, S.D. McDonald, J.W. Zindel, and L.M. Hogan, *Metall. Mater. Trans. A* 32, 949 (2001).
15. Y.H. Cho, H.-C. Lee, K.H. Oh, and A.K. Dahle, *Metall. Mater. Trans. A* 39, 2435 (2008).
16. P. Srirangam, S. Chattopadhyay, A. Bhattacharya, S. Nag, J. Kaduk, S. Shankar, R. Banerjee, and T. Shibata, *Acta Mater.* 65, 185 (2014).
17. M. De Giovanni, J.M.J.M. Warnett, M.A.M.A. Williams, and P. Srirangam, *J. Alloys Compd.* 727, 353 (2017).
18. J. Gröbner, D. Mirković, and R. Schmid-Fetzer, *Metall. Mater. Trans.* 35, 3349 (2004).
19. W.R.T. Ferreira, *ImageJ User Guide IJ 1.46r* (2012).
20. J.H. Li and P. Schumacher, *Int. J. Cast Met. Res.* 25, 347 (2012).

21. M.G. Mahmoud, E.M. Elgallad, M.F. Ibrahim, and F.H. Samuel, *Int. J. Met.* 12, 251 (2018).
22. M.D. Hanna, S. Lu, and A. Hellawell, *Metall. Trans. A* 15, 459 (1984).
23. C.R. Ho and B. Cantor, *J. Mater. Sci.* 30, 1912 (1995).
24. C. Liao, J. Chen, Y. Li, R. Tu, and C. Pan, *J. Mater. Sci. Technol.* 28, 524 (2012).
25. M. Zarif, B. Mckay, and P. Schumacher, *Metall. Mater. Trans. A* 42, 1684 (2010).
26. J.H. Li, X.D. Wang, T.H. Ludwig, Y. Tsunekawa, L. Arnberg, J.Z. Jiang, and P. Schumacher, *Acta Mater.* 84, 153 (2015).
27. J. Barrirero, M. Engstler, N. Ghafoor, N. de Jonge, M. Odén, and F. Mücklich, *J. Alloys Compd.* 611, 410 (2014).
28. J. Barrirero, J. Li, M. Engstler, N. Ghafoor, P. Schumacher, M. Odén, and F. Mücklich, *Scr. Mater.* 117, 16 (2016).
29. M. Timpel, N. Wanderka, R. Schlesiger, T. Yamamoto, D. Isheim, G. Schmitz, S. Matsumura, and J. Banhart, *Ultramicroscopy* 132, 216 (2013).
30. K. Nogita and A. Dahle, *Mater. Charact.* 46, 305 (2001).
31. K. Nogita, A. Knuutinen, S.D. McDonald, and A.K. Dahle, *J. Light Met.* 1, 219 (2001).
32. G. Heiberg and L. Arnberg, *J. Light Met.* 1, 43 (2001).
33. A.K. Dahle, K. Nogita, S.D. McDonald, C. Dinnis, and L. Lu, *Mater. Sci. Eng. A* 413–414, 243 (2005).